LA-UR-79-463

CONF-790143--1

TITLE: ROOM-TEMPERATURE CAVITIES FOR HIGH-BETA ACCELERATING STRUCTURES

AUTHOR(S): S. O. Schriber

SUBMITTED TO: Conference on Future Possibilities for Electron Accelerators, Charlottesville, VA, January 8-10, 1979

University of California

LOS ALAMOS SCIENTIFIC LABORATORY
Post Office Box 1663 Los Alamos, New Mexico 87545
An Affirmative Action/Equal Opportunity Employer

ROOM-TEMPERATURE CAVITIES FOR HIGH-BETA ACCELERATING STRUCTURES

S. O. Schriber*
ACCELERATOR TECHNOLOGY DIVISION
Los Alamos Scientific Laboratory
Los Alamos, New Mexico 87545

SUMMARY

Properties of several room-temperature cavities for standing-wave linear accelerator structures are discussed. In particular, new results related to the disk-and-washer geometry are presented. Extensive calculations using the computer program SUPERFISH have shown that for $\beta = 1.0$ the effective shunt impedance is at least 20% higher than that of an equivalent LAMPF cavity, while quality factors can be a factor of two higher.

INTRODUCTION

Considerable development work on rf accelerating structures has been undertaken because of the need to accelerate proton beams to energies in excess of 200 MeV. The basic goals of this development have been to improve rf efficiency and to simplify assembly and fabrication. For heavily beam loaded systems, studies to reduce beam breakup from higher order modes, to stabilize rf accelerating fields along the length of the structure and to determine effective coupling schemes have also been important. The need for accelerating structures which are efficient converters of rf power to useful beam power is not limited to the acceleration of heavy particles such as protons. Developments in proton linac technology are directly applicable to electron accelerating structures. In particular, high rf efficiency is very important for electron linacs which will be operated continuous wave. Advantages of several room-temperature standing-wave accelerating structures for electron linac applications are discussed in terms of rf properties. Mechanics, cooling, assembly methods and engineered systems are not discussed here, however the selection of cavity geometries considered has had to account for mechanical and cooling constraints.

Since advantages and optimization of the coupled cavity geometry used for LAMPF at LASL have been discussed previously only two salient features will be repeated. For more details the reader is referred to the literature.[1,2] Optimization of the standing-wave cavity geometry led to a superior efficiency in converting rf power to useful beam power. This is illustrated in Fig. 1 which shows curves of effective shunt impedance, ZT^2, at 1.35 GHz as a function of the gap to length, g/L, ratio for particle

*Visitor from Chalk River Nuclear Laboratories, Chalk River, Ontario, Canada KOJ1JO

betas, β , from 0.4 to 1.0. As reported earlier,[3] ZT^2 ranges from 39 to 69 MΩ/m for β from 0.4 to 1.0, respectively. Figure 2a shows dimensional parameters which define the LASL structure geometry. Parameters associated with the nose or drift tube (g, R_H, R_N and Θ) have the largest effects on ZT^2. The web radius, R_3, has a small effect on ZT^2. R_3 can be reduced to zero with only a few percent loss in ZT^2 - for β = 0.8, a 7% loss in ZT^2 is associated with a 7% decrease in R_C. Losses in ZT^2 from surface finish can be larger than this. Advantages in reducing R_3 are a smaller overall radius R_C and a longer straight web with thickness t_w that could be used for coupling slots. The radius R_3 need not be a radius but could be an angled face. Having a smaller overall cavity radius without significantly affecting ZT^2 could be important for some applications requiring circulating beams such as racetrack microtrons. Effects associated with one point multipactor for structures operated 100% duty factor should be considered in the geometry choice when R_3 approaches zero.

Another important aspect of the LASL structures, associated with a suitable coupling scheme, was the choice of the $\pi/2$ mode as the operating mode with all its inherent stabilizing properties.[4,5] Accelerating cavities were rf coupled by side-couplers mounted off-axis - alternate side-couplers being displaced 180° about the beam axis. Other means to rf couple the accelerating cavities are by ring-couplers[6] and by on-axis couplers,[7] always with minimum rf excitation in the coupling cavity for $\pi/2$ mode operation. The degree of $\pi/2$ mode stabilization is directly related to the square of the rf coupling constant between adjacent cavities - the larger the coupling constant, the more insensitive the structure is to tuning, mechanical and assembly errors. Coupling constants of ∿5% have been measured with side-coupled structures while at least 10% has been achieved with ring-coupled and on-axis coupled structures.

An interesting variant of the side-coupled structure is the interlaced side-coupled system described by Vaguine.[8] This structure would be of interest for applications requiring high accelerating gradients without adversely affecting effective shunt impedance.

Reducing intercavity coupling of TM_{110}-like modes is important for heavily beam-loaded structures. This can be achieved in a side-coupled structure by locating alternate side-couplers 90° with respect to the beam axis rather than the usual 180°. With a ring-coupled or an on-axis coupled structure adjacent pairs of coupling slots can be rotated by 90°. Because the quality factor, Q, of the on-axis coupling cavity is ten times smaller than that of the accelerating cavity, most higher order modes will be "Q-spoiled" in an on-axis coupled structure - an important feature basic to the structure geometry.

An on-axis coupled structure has a slightly lower calculated ZT^2 than structures with off-axis couplers because the on-axis coupler takes up space on axis. However, measurements[9] have demonstrated that higher ZT^2 can be obtained with on-axis coupled structures - 95% of calculated ZT^2 can be attained, to be compared with 85% for side-coupled structures. The difference

can be explained partially by the fact that rf losses associated with the coupler were included only in calculations for the on-axis coupled structure. A comparison of calculated ZT^2 at 3 GHz as a function of beta is shown in Fig. 3 - the on-axis coupled ZT^2 is lower by $\sim$4% for $\beta = 1.0$.

Comparing the three types of coupling, the on-axis coupled structure has two advantages - ease of fabrication related to all coaxial components and smaller overall radius because the couplers do not extend beyond the accelerating cavity radius. Advantages of the so-called disk-and-washer geometry shown in Fig. 2b are described in more detail in the following discussions.

Results presented below are limited to axially symmetric structures since calculations could be done with relative ease using the computer program SUPERFISH.[10]

ON-AXIS COUPLED STRUCTURE

Figure 4 illustrates two aspects of a 3 GHz on-axis coupled structure determined from SUPERFISH calculations. Coupling slots were approximated by a narrow annular ring positioned as far as possible from the axis on the flat portion of the web. Figure 4a shows that ZT^2 is linearly related to the coupling constant, being $\sim$6% smaller for 10% coupling and $\sim$12% smaller for 18% coupling. ZT^2 plotted as a function of web thickness in Fig. 4b for a $\beta = 1.0$ cavity exhibits a "shoulder" for thin webs before decreasing linearly. A web thickness of 0.4 cm as described in reference 9 results in a 2% loss in ZT^2.

Calculations to determine the optimum coupling slot location have shown that the coupling slot should be on the flat portion of the web and as far as possible from the axis. This location leads to the largest coupling constant and largest ZT^2. Intercavity coupling was proportional to the square root of slot width and decreased by a factor of three as the slot position moved closer to the beam axis (but constrained to be on the flat portion of the web).

DISK AND WASHER STRUCTURE

Introduction of the disk-and-washer structure[6,11] led to much interest in its rf properties [12,13] because of the much larger rf coupling constant ($\sim$ 50%) and because it appeared to simplify fabrication and assembly of high energy accelerating structures. A further study of the structure by parameterizing the geometry was warranted to determine tolerance information, washer support effects and tuning characteristics. This study using SUPERFISH showed that ZT^2 of the disk-and-washer structure, DAW, could be increased substantially over that previously reported by suitable geometry choice. The two most significant geometrical changes which increased ZT^2 were an increase in the thickness of the disk, t_D, and an increase in the outer radius, R_C. To understand these improvements, the disk-and-washer structure can be considered as a ring-coupled structure which has the slot area completely open. Increasing R_C and t_D alters the rf field distribution and this change reduces power losses in the coupling cavity region - particularly on the outer cylinder.

Optimization of the new DAW geometry used the following procedure. The cavity was considered made of three parts - washer, disk and outer cylinder with relevant geometrical quantities illustrated in Fig. 2b. For a fixed outer cylinder radius, frequencies of the $\pi/2$ accelerating mode, $\pi/2A$, and the $\pi/2$ coupling mode, $\pi/2C$, were made equal by adjusting radii of the washer and the disk, respectively. The disk thickness giving highest ZT^2 was determined from a plot of ZT^2 versus $t_D - R_W$ and R_D being adjusted for each t_D value to maintain $\pi/2A = \pi/2C = 1.35$ GHz. The plot was a shallow function at the peak indicating that t_D could be adjusted to meet mechanical restraints. Using this optimized t_D, the gap, g, which yielded highest ZT^2 was determined from a plot of ZT^2 versus g - again R_W and R_D being adjusted for each g value to maintain $\pi/2A = \pi/2C = 1.35$ GHz. The plot of ZT^2 versus g was a steep function at the peak suggesting tight tolerances for g. The procedure described above was repeated for particle betas from 0.4 to 1.0 to determine optimum t_D and optimum g as a function of beta. It was found that optimum t_D and g were essentially independent of R_C and were therefore fixed for each beta.

Calculations and Geometrical Choices

Figure 5 shows ZT^2 as a function of R_C for particle betas from 0.4 to 1.0. Effective shunt impedances for $\beta = 0.4$, 0.6 and 0.8 geometries have reached a maximum of 34, 59 and 81 MΩ/m, respectively for R_C shown. ZT^2 for $\beta = 1.0$ geometry reaches a maximum of 115 MΩ/m for a larger R_C than shown -a ZT^2 1-2/3 times that of an equivalent LASL cavity. Reasons for not choosing large R_C values will be explained later. Higher effective shunt impedances than were previously reported can be obtained and these improvements pertain to a washer geometry which does not have a knob at its outer radius. Calculations are underway which indicate that further improvements in ZT^2 can be obtained for $\beta = 0.4$ to 0.6 geometries by the addition of a suitably shaped knob.

Table 1 lists parameters for the $\beta = 1.0$ geometry calculations associated with Fig. 5. Results are normalized to an average on-axis accelerating field of 1 MV/m. As R_C increases, the percent rf losses on the disk and the cylinder decrease which is related to changes in the $\pi/2A$ mode field distribution. Maximum electric fields on the surface decrease by $\sim 1.5\%$, quality factor, Q, increases by a factor of three, and ZT^2 increases by a factor of two as R_C increases from 10.84 to 19.84 cm. Geometrical quantities not specified in the body of the table are listed in the heading. Figure 6 shows radii of the disk and the washer as a function of R_C for the range of beta associated with the curves plotted in Fig. 5. Other geometrical parameters for cavities with betas other than 1.0 are the same as those listed in the heading of Table 1 for $\beta = 1.0$ except that L, t_D and g are different - the last two quantities should be obtained from Fig. 9, $L = \beta\lambda/4$.

Figure 6 shows that radii of the disk and the washer overlap at $R_C \sim 16$ cm for $\beta = 0.4$ and at $R_C \sim 12$ cm for $\beta = 1.0$. For R_C less than these values there is a complete overlapping of radii with no direct line of

sight down the structure when viewed from the end. Alternatively, for larger R_C there is a direct line of sight which improves vacuum conductance and which could lead to more varied and possibly simpler assembly methods. It should be noted that a particular R_C can be chosen for all beta resulting in a linear accelerator with a constant outer diameter.

Although larger R_C leads to higher ZT^2, reasons illustrated in Fig. 7 lead to a practical upper limit for the outer cylinder radius of a DAW structure. In certain applications such as for structures with a small number of cavities the arguments given below can be overcome by suitable geometry choice. Figure 7 shows frequency dispersion curves for $\beta = 1.0$ geometries at four selected values of R_C ranging from 10.84 to 19.84 cm. The dispersion curve would be almost symmetric about the 1.35 GHz $\pi/2A$ mode when $R_C \simeq 12$ cm (when coincidentally $R_W \simeq R_D$). As R_C increases, second neighbour coupling between coupling cavities increases and this change distorts the dispersion curve so that it is no longer symmetric about the $\pi/2A$ mode. At large values of R_C (for example $R_C = 19.84$ cm) two noticeable properties of the dispersion curve occur, both of which are disadvantageous to structure operation in the $\pi/2A$ mode.

An investigation of the dispersion curve for large R_C between the $\pi/2$ and π modes shows that modes can be excited which result in mode overlapping or interference with the desired $\pi/2A$ mode. Such interference can result in an unacceptable distribution of rf fields along the length of the structure and/or greatly reduced stabilization properties. This degradation of structure performance is clearly undesirable. At the same time the $\pi/2A$ mode group velocity decreases related to changes in slope of the dispersion curve and this negates one of the reasons for choosing the DAW structure - that of a large coupling constant and the usually associated high group velocity. Nonlinear least squares fits of the calculated frequencies to the dispersion relationship for an R-L-C loop-coupled model yielded coupling constants between accelerating and coupling cavity, between adjacent accelerating cavities and between adjacent coupling cavities which varied from 0.6 to 0.4, -0.2 to 0.1 and 0.1 to 0.6, respectively, as R_C changed from 10.84 to 19.84 cm.

Similar frequency dispersion curve behavior was noted for $\beta = 0.4$, 0.6 and 0.8 geometries suggesting that R_C should not exceed 17 cm at 1.35 GHz. Dispersion curves were symmetric about the $\pi/2A$ mode when $R_C \simeq 12$ cm for all beta. Fits to the frequency data showed that the set of coupling constants were almost identical to those of another beta geometry with the same R_C. This result is surprising because R_W and R_D differ for different betas with the same R_C. It would be expected that the different overlapping of rf fields would produce different sets of coupling constants.

A recent survey calculation has shown that high ZT^2 for a $\beta = 1.0$ geometry with large R_C (i.e., > 20 cm) might be possible for a long structure without mode interference and with high group velocity. A solid annular ring with coupling slots could be used to support the washer from the outer cylinder. The effect of the annular ring is to reduce second neighbor coupling leading to a more acceptable dispersion curve. Tradeoff between rf losses on the annular ring and the size of the coupling slot is still to be determined.

"Harmonic Accelerator"

Frequency dispersion curves for the four lowest passbands which have axial symmetric mode patterns are shown in Fig. 8 for the $\beta = 0.6$ geometry with $R_C = 16.6$ cm. The $\pi/2A$ mode of each passband has a field distribution similar to that of the first passband in the region which can be occupied by beam. An R_C value exists for each beta geometry which makes the frequency of an upper passband $\pi/2A$ mode exactly twice the frequency of the first passband $\pi/2A$ mode. Such an accelerating structure can then be excited at two frequencies - one twice the other. With proper phasing and amplitude control the time rf field variation can be made closer to linear especially during the time that the beam longitudinal phase bucket passes the cavity gap (the first two terms in the fourier series for a sawtooth wave are represented, $\sin(wt) - \sin(2wt)/2$. Operation of this "harmonic accelerator" with beam should reduce the transverse emittance growth normally associated with a sinusoidal variation of rf field across a gap. Optimum values for the harmonic content as a function of phase spread and stable phase angle have been determined by Crandall.[14]

The second passband satisfies the "harmonic accelerator" conditions for $\beta = 0.6$ geometry when $R_C = 14.7$ cm. Calculated Z for the harmonic mode is approximately one half that of the fundamental. The "harmonic accelerator" conditions are satisfied for $\beta = 1.0$ geometry by the third passband when $R_C = 17.1$ cm. For this choice the calculated Z for the harmonic mode is approximately one quarter that of the fundamental. The criterion used to select a specific passband for the harmonic mode was based on keeping ZT^2 of the fundamental mode as high as possible without having too large an R_C. The second passband mode could have been used for the $\beta = 1.0$ geometry, however R_C would have to be less than 10 cm with a much smaller ZT^2.

Stored Energy Mode

Tables 2 and 3 give relevant parameters of the $\beta = 0.6$ and 1.0 geometries related to optimizing the gap g. The last row of numbers for each table corresponds to a geometry without a drift tube nose. As expected with increasing g, Q increases, ZT^2 peaks and E_{max} decreases. A linear accelerator operating in the stored energy mode should employ cavities with a large gap for most efficient operation. Using Q/ZT as a comparison guide for stored energy applications the DAW geometry for g/L = 0.937 given in Table 3 is two times better than an equivalent LASL cavity.

PIGMI Geometry

The DAW geometry chosen for PIGMI[15] had to meet specific mechanical constraints for a structure operating at 1.32 GHz. An R_C value of 16.6 cm was chosen for all beta to ensure that the problems discussed above would not be encountered and to be compatible with available pipe size. A thicker washer web (0.4 cm) was required for internal cooling channels, a support knob was required on the washer extremity for mounting radial stems which support the washer from the outer cylinder, and a slightly larger beam bore hole was

required to match jigging that would be used to support the washer during brazing operations. Data for the 1.32 GHz geometries selected for PIGMI are given in Table 4. A least squares fit of ZT^2 versus β to a polynomial gives the following expression where f is in GHz

$$ZT^2(M\Omega/m) = \sqrt{f}\,(-60.53\beta^2 + 161.47\,\beta - 26.60) \quad ,$$

an expression accurate to within 0.2 $M\Omega/m$ at 1 GHz from $\beta = 0.4$ to 1.0. Dimensions given in Table 4 must be scaled appropriately to use the ZT^2 expression for frequencies other than 1.32 GHz.

Figure 9 gives the disk radius, washer radius, gap and disk width as a function of β for the optimized 1.32 GHz geometry with R_C = 16.6 cm. It should be noted that the outer cylinder radius selected is similar to the overall outer radius of a side-coupled structure when the space occupied by the side-coupler is included ($\sim$16.5 cm).

A ZT^2 comparison of the DAW geometries listed in Tables 1 and 4 and equivalent LASL cavities is shown in Fig. 10. The DAW geometry has a higher ZT^2 for betas greater than 0.6. Since calculations for the DAW geometry included the rf losses in the coupling cavities it is expected that experimental results will show a greater difference in favour of the DAW geometry than that illustrated in Fig. 10.

Fabrication of the outer cylinder from stainless steel 304 instead of copper reduces the Q of the $\pi/2A$ mode by only 6% for the $\beta = 1.0$ geometry but reduces the $\pi/2C$ mode Q by a factor of almost 7. This is an interesting way to build the DAW structure when "Q-Spoiling" of higher order modes is a desireable feature. Similar results can be obtained if the outer cylinder is coated with a lossy material such as nichrome.

Frequency and ZT^2 sensitivities of the β = 0.6 and 1.0 PIGMI cavities to geometrical changes are given in Table 5. Fractional increase in ZT^2 related to gap changes is mainly from frequency changes of the $\pi/2$ mode. Improvements in ZT^2 can be made by a thinner washer web and a smaller bore hole radius. The table is useful to determine what geometrical parameter should be used for tuning the $\pi/2A$ and $\pi/2C$ modes. The most efficient means to tune the $\pi/2A$ mode is to change R_W or g with g favoured for mechanical reasons. Similarly, changes to R_D and R_C are preferred to tune the $\pi/2C$ mode with R_D favoured for mechanical reasons.

Graded-Beta Structure

A graded-beta accelerating structure can be fabricated easily using the DAW geometry because a constant outer cylinder radius can be selected for all beta. Termination of the structure can be with a half cavity, with a full cavity or with a full cavity joined to a coaxial coupler excited by a TEM-like mode distribution as shown in Fig. 11a, b and c, respectively. The full cavity termination has the lowest rf losses of the three types of termination when normalized to the same cavity energy gain. The coaxial coupler can also be used as the means to couple to an external rf source.

Dimensions for the washer and the disk change along the length of the structure to ensure that each cavity has the required rf properties. A least squares fit to calculated results from different graded-beta geometries consisting of two cavities yielded the following expression for the average axial electric field, E_i, of the ith cavity

$$E_i/E_{i+1} = 0.8(L_{i+1}/L_i) + 0.2$$

where L_i is the length of the ith cavity as defined in Fig. 2. Figure 12 shows the cavity geometry for graded beta structures composed of a $\beta = 0.4$ to 0.6 combination and a $\beta = 0.4$ to 1.0 combination. Criteria used to select the geometry shown in Fig. 12 were

a) The geometry close to axis including the drift tube nose on the washer was made symmetric about the gap center for each cavity.

b) Washer and disk dimensions corresponding to the cavity betas were used to first order with small changes in the washer and disk radii to keep $\pi/2A = \pi/2C$.

Changing t_D was the best method found to compensate for differences in average on-axis electric fields between adjacent accelerating cavities because frequency changes to the $\pi/2A$ and $\pi/2C$ modes were minimized. A 44% change in t_D resulted in a 10% change in the on-axis fields for both the $\beta = 0.6$ and 1.0 geometries with the lower (higher) field occurring below the disk which had been shortened (increased). This method can be used to compensate for changes in on-axis fields related to the use of washer supports which are not located symmetrical to the central plane of the washer. Changes in t_D for every accelerating cavity and/or the use of non-symmetrical washer supports will result in a frequency dispersion curve which is quadruperiodic in nature rather than biperiodic. Gaps in the passband will appear at $\pi/4$ and $3\pi/4$ associated with a degeneracy for these modes.

DISCUSSION AND CONCLUSIONS

Excluding the disk-and-washer geometry, the on-axis coupled geometry should have the highest ZT^2 in practice. Additional advantages accrue from the coaxial configuration - relatively small outer diameter and simplified assembly procedures. Calculations have demonstrated that the coupling slot should be as distant from the beam axis as possible to yield high ZT^2 and large coupling constant. For applications imposing a constraint on the outer radius of the accelerating structure, the on-axis coupled structure would be be preferred to a disk-and-washer geometry when $R_C < 13$ cm (at 1.35 GHz) for $\beta = 0.8$ and when $R_C < 12$ cm (at 1.35 GHz) for $\beta = 1.0$ because of a higher ZT^2.

The interlaced side-coupled structure introduced by Vaguine[8] can be used for applications requiring high accelerating gradients but not at the expense of a loss in ZT^2. An inspection of Table 3 and Fig. 10 shows that high accelerating gradients can be attained with a larger ZT^2 than the interlaced side-coupled structure when a large gap geometry is selected for a $\beta = 1.0$ disk-and-washer structure - accelerating gradients of 40 MeV/m at 3 GHz should be possible with a 20% safety factor.

Geometries for a DAW system have been determined which yield higher ZT^2 than reported earlier - up to 20% higher than an equivalent LASL cavity. Higher ZT^2's are possible, up to 66% higher, but these geometries would not be practical for most applications. Uncertainties associated with non-axially-symmetric higher-order modes and with effects of the washer supports need to be resolved. Models of the $\beta = 0.6$ and $\beta = 1.0$ geometries will be tested at LASL shortly to check the calculations and to determine if any unexpected phenomenum occur.

A DAW structure geometry can be selected to have a mode at twice the operating frequency which has an on-axis field distribution similar to that of the operating mode. Operation of this "harmonic accelerator" with rf drives at the two frequencies (being properly controlled in phase and amplitude) should result in a structure which exhibits a reduced growth in the transverse beam emittance.

The disk-and-washer geometry lends itself to graded-beta linacs such as those for electron injectors. Average on-axis field changes from cavity-to-cavity are tolerable and can be controlled to some extent by changes in the disk thickness. Terminating the structure in a coaxial coupler operating in a TEM-like mode seems natural and can offer an extra advantage by serving as the means to couple to an external rf source.

The new disk-and-washer geometry has many advantages over other geometries suitable for room-temperature standing-wave linacs. Experimental verification of the improved properties and a determination of aspects not predictable by SUPERFISH are required and should be completed soon.

ACKNOWLEDGMENTS

The author would like to thank T. J. Boyd, Jr., J. M. Potter, D. A. Swenson and L. Wilkerson for their participation in interesting discussions related to this work and for their interest in its overall implications and constraints.

REFERENCES

1. H. C. Hoyt, D. D. Simmons and W. F. Rich, Computer Designed 805 MHz Proton Linac Cavities, Rev. Sci. Instr. 37, 755 (1966).
2. E. A. Knapp, B. C. Knapp and J. M. Potter, Standing Wave High Energy Linear Accelerator Structures, Rev. Sci. Instr. 39, 979 (1968).
3. J. J. Manca and E. A. Knapp, TM_{01} Mode Accelerating Cavity Optimization, Los Alamos Scientific Laboratory Report No. LA-7323 1978).
4. J. E. Nagle and E. A. Knapp, Steady State Behaviour of a Ring or a Chain of Coupled Circuits, Proc. of Conf. on Proton Linacs at Yale University, TID-7691, 171 (1963).
5. G. E. Lee-Whiting, Analysis of Equivalent Circuits of Linac Tanks, Proc. of 1968 Proton Linac Conf., Brookhaven National Laboratory Report No. BNL-50120, 471 (1968).
6. V. G. Andreev et al., Study of High-Energy Proton Linac Structures, Proc. of 1972 Proton Linac Conf., Los Alamos Scientific Laboratory Report No. LA-5115, 114 (1972).

7. S. O. Schriber, E. A. Heighway and L. W. Funk, Beam Tests with S-Band Standing Wave Accelerators Using On-Axis Couplers, ibid., 140 (1972).
8. V. A. Vaguine, Standing Wave High Gradient Accelerator Structure, IEEE Trans, Nucl. Sci., NS-24, 1084 (1977).
9. S. O. Schriber, L. W. Funk and R. M. Hutcheon, Effective Shunt Impedance Comparison between S-Band Standing Wave Accelerators with On-Axis and Off-Axis Couplers, Proc. of 1976 Proton Linac Conf., Atomic Energy of Canada Limited Report No. AECL-5677, 338 (1976).
10. K. Halbach, R. F. Holsinger, W. E. Jule and D. A. Swenson, Properties of the Cylindrical RF Cavity Evaluation Code SUPERFISH, ibid., 122 (1976).
11. V. G. Andreev et al. Investigation of the Accelerating Stucture for the Second Part of the Meson Factory Linac, ibid., 269 (1976).
12. J. J. Manca, E. A. Knapp and D. A. Swenson, High Energy Accelerating Structures for High Gradient Proton Linac Applications, IEEE Trans. Nucl. Sci., NS-24, 1087 (1977).
13. J. J. Manca and E. A. Knapp, Optimization of the Disk and Washer Accelerating Cavities, Los Alamos Scientific Laboratory Report No. LA-7407 (1978).
14. K. R. Crandall, Transverse Emittance Increase in an RF Gap: Reduction of Effect by Addition of Harmonic, private communication (1978).
15. E. A. Knapp and D. A. Swenson, The PIGMI Program at LASL, Proc. of 1976 Proton Linac Conf., Atomic Energy of Canada Limited Report No. AECL-5677, 230 (1976).

TABLE 1

Parameters for the Disk-and-Washer (1.35 GHz)
as a Function of the Outer Radius, R_C

($\beta = 1.0$, $t_D = 2.65$ cm, $t_W = t_R = 0.35$ cm, $R_H = 1.1$ cm,
$R_N = 0.25$ cm, $R_R = 0$, $\theta = 30°$, $L = 5.555$ cm)

R_C(cm)	R_D(cm)	R_W(cm)	ZT^2(MΩ/m)	T	Q	Emax on surface (MV/m)	% Power on Metal Walls Cylinder	Disk	Washer
10.84	7.50	10.06	49.83	0.812	22369	4.02	6.7	36.1	57.2
11.84	8.96	9.50	66.71	0.813	32215	3.98	2.4	32.7	64.9
12.84	10.25	9.10	74.88	0.813	40179	3.97	1.5	29.1	69.4
13.84	11.46	8.93	80.14	0.813	46962	3.97	1.3	25.9	72.8
14.84	12.63	8.84	84.25	0.813	53033	3.97	1.2	23.2	75.6
15.84	13.77	8.78	87.70	0.813	58577	3.96	1.2	20.9	77.9
16.84	14.90	8.73	90.61	0.813	63671	3.96	1.2	18.9	79.9
17.84	16.01	8.70	92.69	0.814	68355	3.94	1.2	17.3	81.5
18.84	17.10	8.67	95.06	0.813	72746	3.96	1.2	15.9	82.9
19.84	18.19	8.65	96.86	0.813	76827	3.96	1.2	14.6	84.2

TABLE 2

Parameters for the Disk and Washer (1.35 GHz)
as a Function of the g/L Ratio

($\beta = 0.6$, $R_C = 15.45$ cm, $t_D = 0.9$ cm, $t_W = t_R = 0.35$ cm,
$R_H = 1.1$ cm, $R_N = 0.25$ cm, $R_R = 0$, $\theta = 30°$, $L = 3.33$ cm)

g/L	R_D(cm)	R_W(cm)	ZT^2(MΩ/m)	T	Q	Emax on surface (MV/m)	% Power on Metal Walls		
							Cylinder	Disk	Washer
0.282	11.35	9.37	50.54	0.898	25,955	6.15	0.03	2.2	97.8
0.376	11.36	10.07	56.25	0.872	28,174	5.04	0.06	4.0	95.9
0.414	11.37	10.30	56.91	0.860	28,902	4.71	0.07	4.8	95.1
0.470	11.38	10.59	56.08	0.841	29,732	4.29	0.09	6.0	93.9
0.564	11.40	10.97	51.88	0.808	30,652	3.71	0.14	8.1	91.8
0.658	11.42	11.23	45.89	0.776	31,123	3.22	0.20	9.7	90.1
0.895	11.42	11.52	33.02	0.734	31,283	1.94	0.24	12.0	87.8

TABLE 3

Parameters for the Disk and Washer (1.35 GHz)
as a Function of the g/L Ratio

($\beta = 1.0$, $R_C = 16.75$ cm, $t_D = 2.65$ cm, $t_W = t_R = 0.35$ cm,
$R_H = 1.1$ cm, $R_N = 0.25$ cm, $R_R = 0$, $\theta = 30°$, $L = 5.555$ cm)

g/L	R_D(cm)	R_W(cm)	ZT^2(MΩ/m)	T	Q	Emax on surface (MV/m)	% Power on Metal Walls		
							Cylinder	Disk	Washer
0.360	14.91	7.28	66.84	0.910	49324	5.92	0.8	11.6	87.6
0.480	14.84	8.11	82.80	0.861	55682	4.58	1.0	14.8	84.2
0.582	14.80	8.74	90.13	0.814	62986	4.16	1.2	19.0	79.8
0.600	14.79	8.82	90.41	0.805	64572	3.79	1.3	19.9	78.8
0.719	14.75	9.32	87.23	0.750	72546	3.29	1.5	25.1	73.4
0.839	14.73	9.59	77.17	0.712	77223	2.52	1.7	28.7	69.6
0.937	14.73	9.68	70.67	0.707	78515	1.61	1.8	29.8	68.4

TABLE 4

Parameters for the Disk and Washer (1.32 GHz)
as a Function of Beta

(R_C = 16.6 cm, t_W = 0.4 cm, t_R = 1.11 cm, R_H = 1.111 cm,
R_N = 0.25 cm, R_R = 0.476 cm, θ = 30°)

eta	R_D(cm)	R_W(cm)	t_D(cm)	g/L	L(cm)	ZT^2(MΩ/m)	T	Q	Emax on surface (MV/m)	% Power on Metal Walls: Cylinder	Disk	Washer
0.4	11.81	10.71	0.36	0.306	2.271	32.40	0.852	18,253	5.33	0.0012	0.70	99.3
0.5	12.15	10.48	0.61	0.360	2.839	44.99	0.862	23,213	5.05	0.0083	1.25	98.74
0.6	12.54	10.25	0.92	0.415	3.407	55.76	0.861	28,233	4.65	0.032	2.16	97.81
0.7	12.93	9.97	1.30	0.460	3.975	65.09	0.854	33,404	4.50	0.088	3.59	96.32
0.8	13.38	9.64	1.72	0.504	4.542	73.11	0.843	39,191	4.34	0.21	5.93	93.86
0.9	13.90	9.26	2.20	0.544	5.110	80.35	0.829	46,548	4.31	0.45	10.09	89.46
1.0	14.59	8.72	2.71	0.582	5.678	85.31	0.814	57,425	4.18	1.14	18.34	80.52

Table 5

Disk and Washer Parameter Sensitivity

(1.32 GHz, R_C = 16.6 cm)

β = 0.6

Parameter (P)	$\Delta f(\pi/2A)/\Delta P$ (MHz/cm)	$\Delta f(\pi/2C)/\Delta P$ (MHz/cm)	$\Delta ZT^2/\Delta P$ (MΩ/m)/cm
Outer Radius (R_C)	3.9	-185	0.4
Disk Radius (R_D)	3.8	195	0.9
Washer Radius (R_W)	-100	-18	-3.7
Gap (g)	161	0.01	5.5
Disk Width (t_D)	-10.5	-17	-0.6
Washer Width (t_W)	135	-0.9	-16.7
Bore Radius (R_H)	-50	-0.01	-30.4

β = 1.0

Parameter (P)	$\Delta f(\pi/2A)/\Delta P$ (MHz/cm)	$\Delta f(\pi/2C)/\Delta P$ (MHz/cm)	$\Delta ZT^2/\Delta P$ (MΩ/m)/cm
Outer Radius(R_C)	3.8	-116	1.7
Disk Radius (R_D)	-6.2	104	0.6
Washer Radius (R_W)	-76	0.9	-3.2
Gap (g)	73	5.0	6.5
Disk Width (t_D)	5.3	21	-0.3
Washer Width (t_W)	45	1.2	-1.0
Bore Radius (R_H)	-28	-2.9	-26.3

FIGURE CAPTIONS

Fig. 1 Etfective shunt impedance, ZT^2, of 1.35 GHz LASL cavity geometry versus the gap to length ratio, g/L, for betas from 0.4 to 1.0.

Fig. 2 Illustration of the LASL structure and the disk-and-washer geometry showing the symbols used to define the various dimensions.

Fig. 3 Comparison of calculated effective shunt impedance, ZT^2, at 3 GHz for a LASL cavity and an on-axis coupled cavity as a function of particle beta.

Fig. 4 Effective shunt impedance, ZT^2, for a 3 GHz on-axis coupled geometry as a function of a) first neighbor coupling constant and b) web thickness, t_W.

Fig. 5 Effective shunt impedance, ZT^2, of the 1.35 GHz disk-and-washer geometry as a function of the outer cylinder radius, R_C, for betas from 0.4 to 1.0.

Fig. 6 Radii of the disk and the washer associated with Fig. 5 versus the outer cylinder radius, R_C, for betas from 0.4 to 1.0.

Fig. 7 Frequency dispersion curves for the $\beta = 1.0$, 1.35 GHz disk-and-washer geometry for different outer cylinder radii, R_C.

Fig. 8 The four lowest passbands of axially-symmetric modes for $\beta = 0.6$, 1.32 GHz disk-and-washer geometry.

Fig. 9 Disk radius, washer radius, gap to length ratio and disk width to length ratio versus beta for the 1.32 GHz disk-and-washer geometry.

Fig. 10 Comparison of calculated effective shunt impedance, ZT^2, at 1.32 GHz for a LASL cavity and two disk-and-washer geometries as a function of particle beta.

Fig. 11 Terminations for the disk-and-washer geometry in a) half cavity, b) full cavity, and c) full cavity with coaxial coupler attached

Fig. 12 Disk-and-washer graded beta geometry for a) $\beta = 0.4$ to 0.6 and b) $= 0.4$ to 1.0.

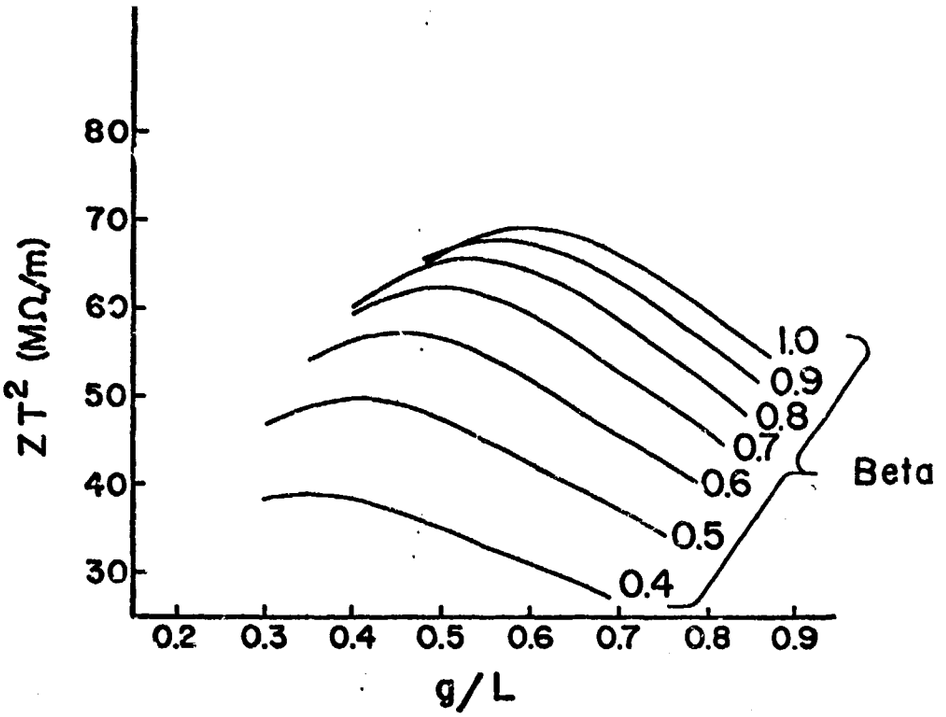

Fig. 1 Effective shunt impedance, ZT^2, of 1.35 GHz LASL cavity geometry versus the gap to length ratio, g/L, for betas from 0.4 to 1.0.

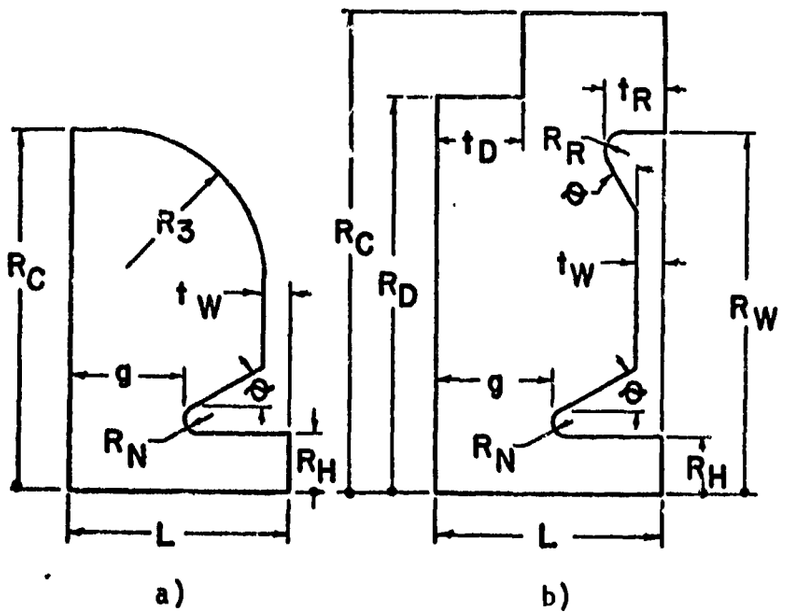

Fig. 2 Illustration of the LASL structure and the disk-and-washer geometry showing the symbols used to define the various dimensions.

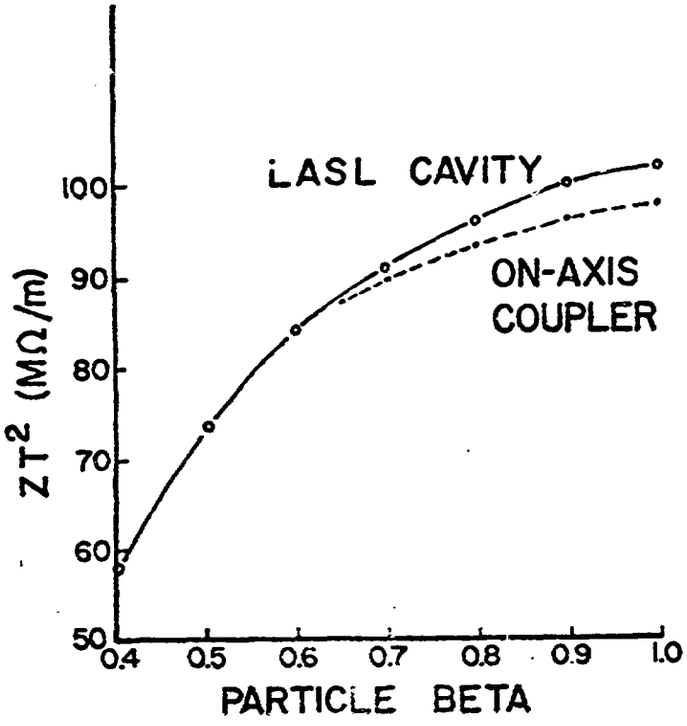

Fig. 3 Comparison of calculated effective shunt impedance, ZT^2, at 3 GHz for a LASL cavity and an on-axis coupled cavity as a function of particle beta.

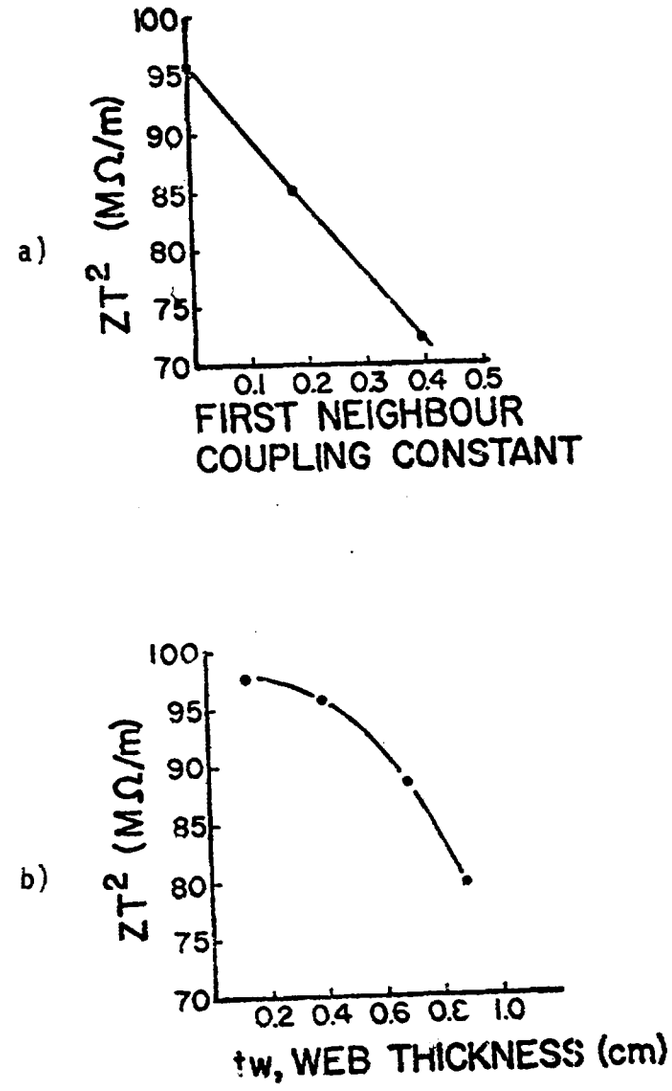

Fig. 4 Effective shunt impedance, ZT^2, for a 3 GHz on-axis coupled geometry as a function of a) first neighbor coupling constant and b) web thickness, t_w.

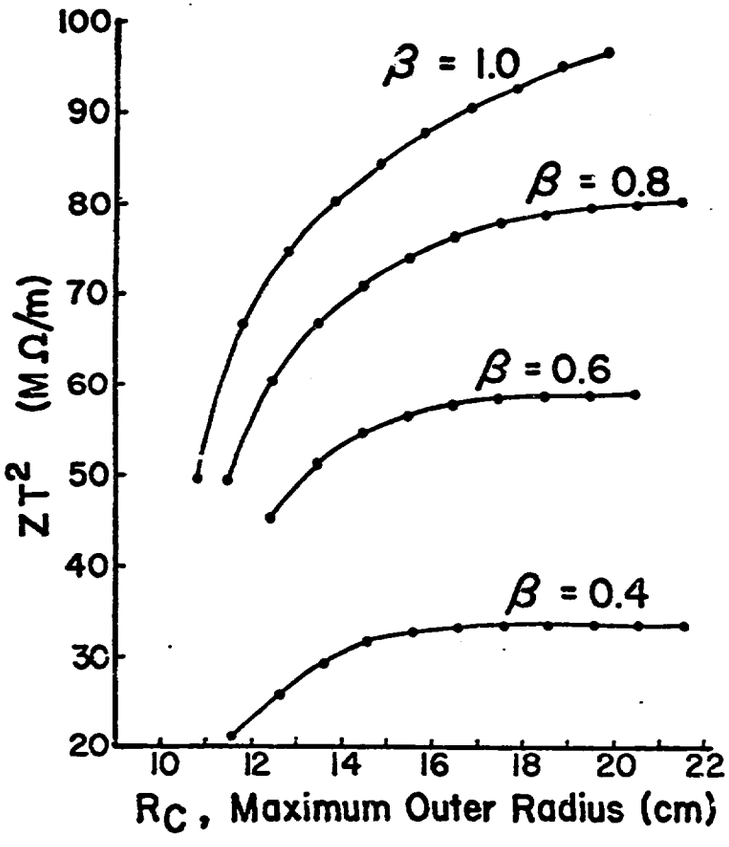

Fig. 5 Effective shunt impedance, ZT^2, of the 1.35 GHz disk-and-washer geometry as a function of the outer cylinder radius, R_C, for betas from 0.4 to 1.0.

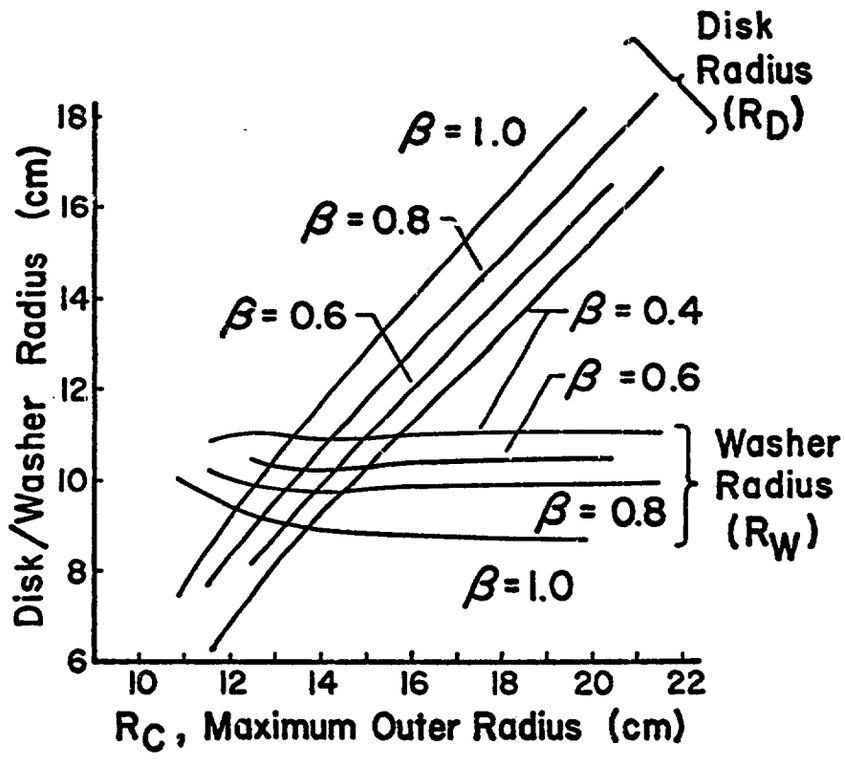

Fig. 6 Radii of the disk and the washer associated with Fig. 5 versus the outer cylinder radius, R_C, for betas from 0.4 to 1.0.

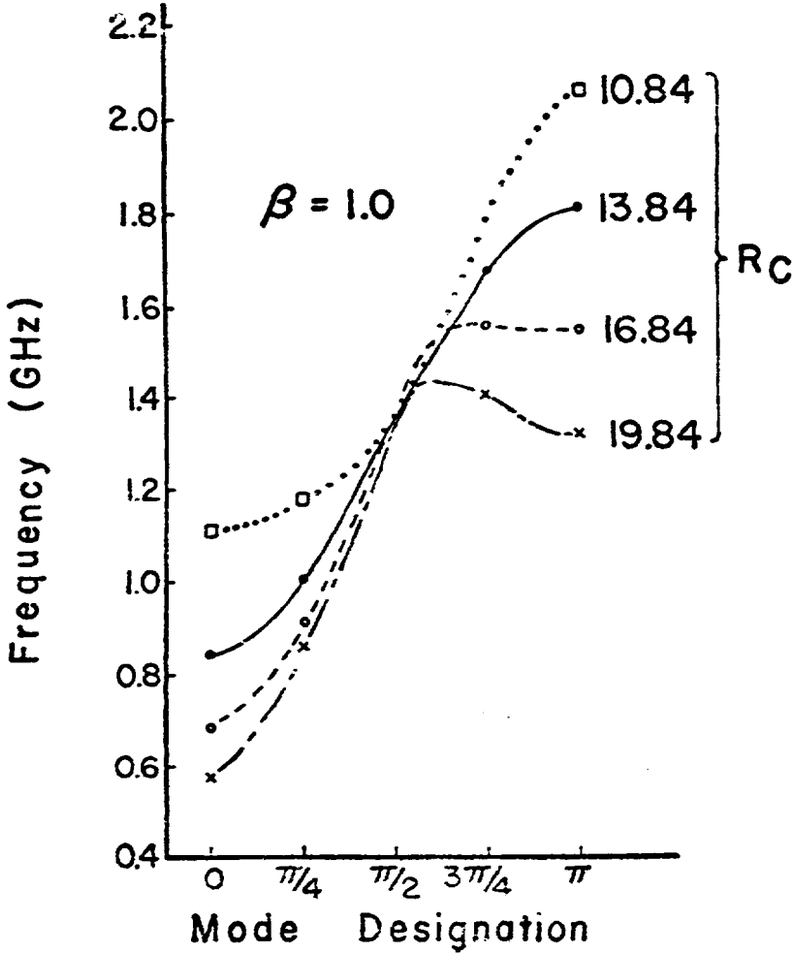

Fig. 7 Frequency dispersion curves for the β = 1.0, 1.35 GHz disk-and-washer geometry for different outer cylinder radii, R_C.

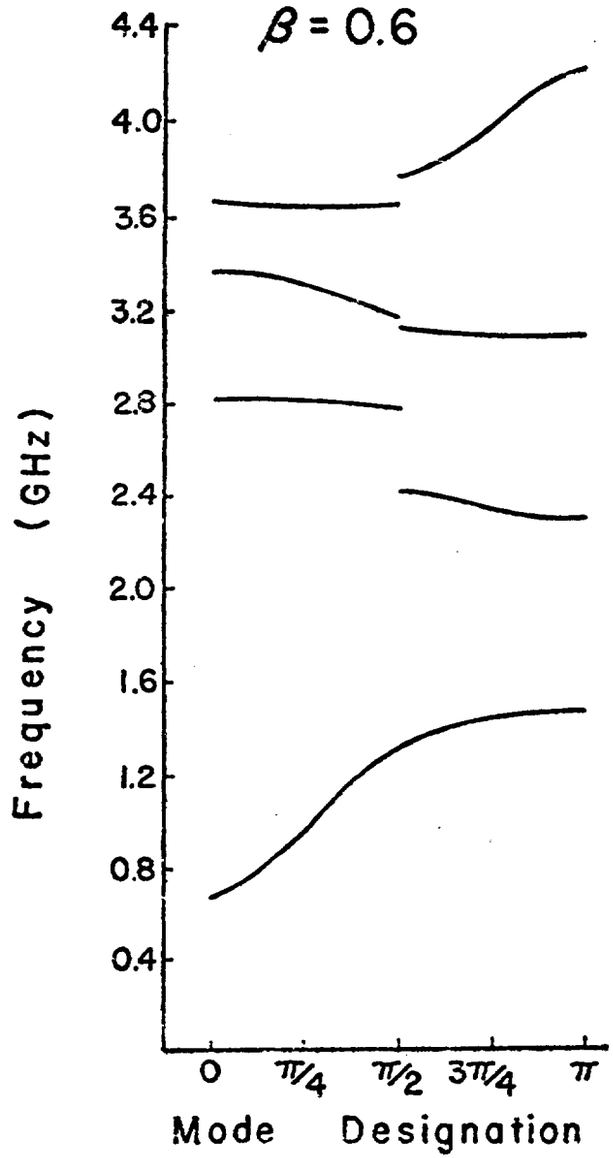

Fig. 8 The four lowest passbands of axially-symmetric modes for β = 0.6, 1.32 GHz disk-and-washer geometry.

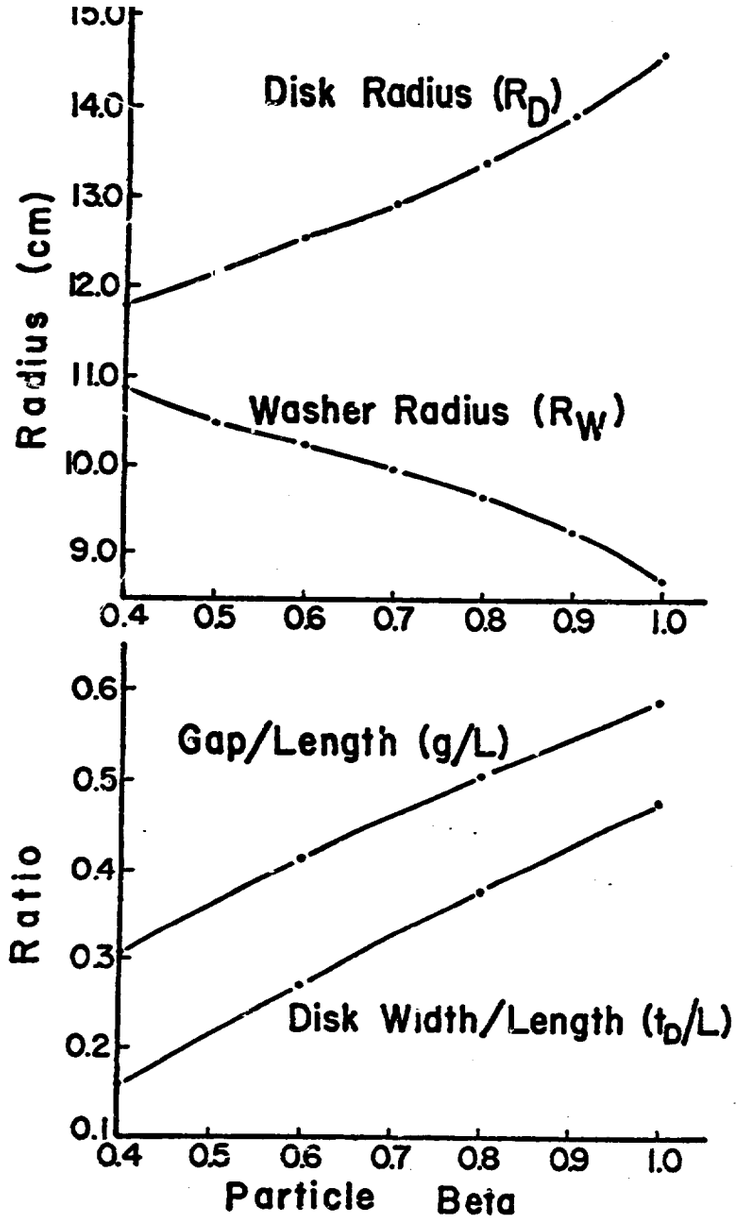

Fig. 9 Disk radius, washer radius, gap to length ratio and disk width to length ratio versus beta for the 1.32 GHz disk-and-washer geometry.

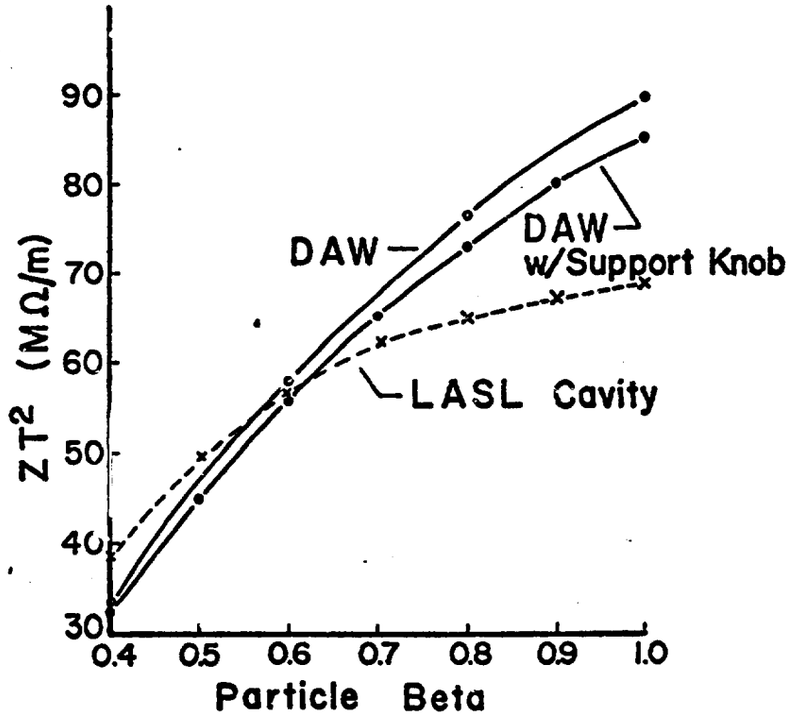

Fig. 10 Comparison of calculated effective shunt impedance, ZT^2, at 1.32 GHz for a LASL cavity and two disk-and-washer geometries as a function of particle beta.

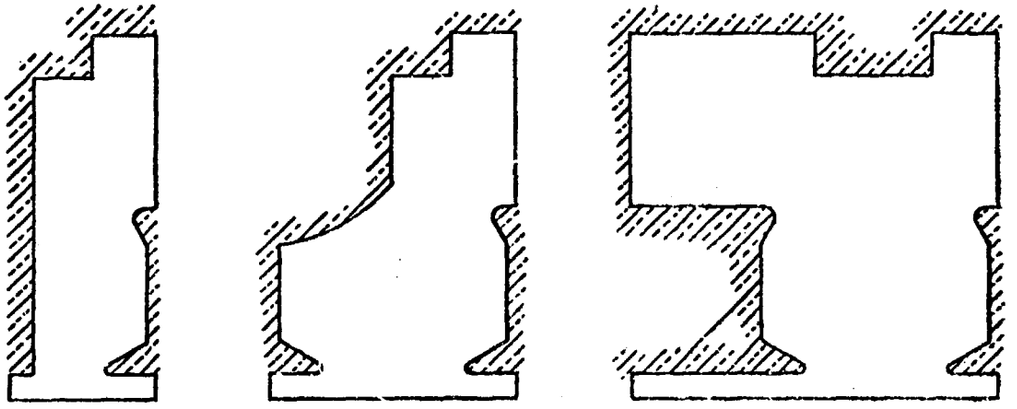

Fig. 11 Terminations for the disk-and-washer geometry in a) half cavity, b) full cavity, and c) full cavity with coaxial coupler attached.

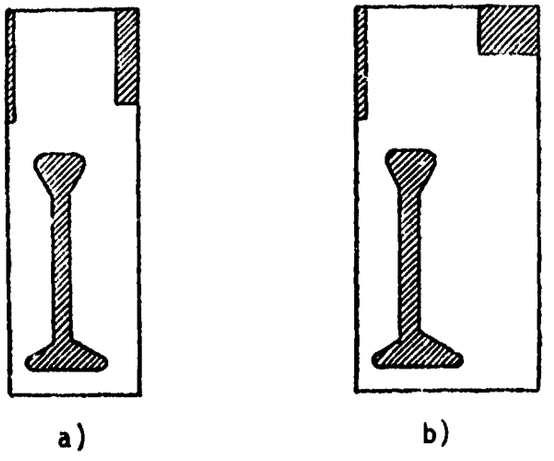

Fig. 12 Disk-and-washer graded beta geometry for a) $\beta = 0.4$ to 0.6 and b) $\beta = 0.4$ to 1.0.